




EASE: Energy-Aware job Scheduling for vehicular Edge networks with renewable energy resources

Giovanni Perin* , *Graduate Student Member, IEEE*,

Francesca Meneghello* , *Member, IEEE*, Ruggero Carli , *Senior*

Member, IEEE, Luca Schenato , *Fellow, IEEE*,

and Michele Rossi , *Senior Member, IEEE*

Abstract

The energy sustainability of multi-access edge computing (MEC) platforms is addressed in this paper, by developing Energy-Aware job Scheduling at the Edge (EASE), a computing resource scheduler for edge servers co-powered by renewable energy resources and the power grid. The scenario under study involves the optimal allocation and migration of time-sensitive computing tasks in a resource-constrained internet of vehicles (IoV) context. This is achieved by tackling, as a main objective, the minimization of the carbon footprint of the edge network, whilst delivering adequate quality of service (QoS) to the end users (e.g., meeting task execution deadlines). EASE integrates a i) centralized optimization step, solved through model predictive control (MPC), to manage the renewable energy that is locally collected at the edge servers and their local computing resources, estimating their future availability, and ii) a distributed consensus step, solved via dual ascent in closed form, to reach agreement on service migrations. EASE is compared with existing strategies that always and never migrate the computing tasks. Quantitative results demonstrate the greater energy efficiency achieved by EASE, which often gets close to complete carbon neutrality, while also improving the QoS.

Index Terms

multi-access edge computing, energy efficiency, green computing networks, mobility management, service migration, distributed scheduling.

All authors are with the Department of Information Engineering, University of Padova, via Gradenigo 6/b, 35131, Padova, Italy.

Michele Rossi is also with the Department of Mathematics “Tullio Levi-Civita”, University of Padova, via Trieste 63, 35121, Padova, Italy.

*Corresponding authors, emails: {name.surname}@dei.unipd.it.

I. INTRODUCTION

The future of cellular networks is not only concerned with faster and more reliable wireless connections. The rapid digitalization of the society – the number of Internet users will grow from 50% to 66% of the world population by 2023 [1] – comes with a need to expedite the service provisioning time, demanding support for *computation-intensive* and *delay-sensitive* users' applications. Often, these applications cannot be executed on the end-devices due to memory and energy scarcity, neither on the network cloud due to a consequent surge in the Internet traffic and to excessive delays. These facts lead to the introduction of the MEC paradigm, entailing the de-location of computation services at the mobile network edge, by empowering the evolved node B (eNB) sites with adequate computing facilities. In a MEC architecture, a user can offload intensive computing jobs to the closer mobile edge host (MEH), thus considerably reducing the communication delays with respect to cloud services. Spurred by the high potential of such innovation, the European Telecommunications Standards Institute (ETSI) is extensively working on the standardization of interoperable MEC architectures [2], along with their integration with fifth-generation (5G) – and beyond – mobile networks [3].

In this work, we focus on an IoV scenario, where the network users are 5G – or beyond 5G – enabled vehicles requiring communication and computing support [4], [5]. According to [1], among machine-to-machine (M2M) communications, connected cars is the vertical with the highest expected compound annual growth rate (30%) until at least 2023. Moreover, as pointed out by [6], one of the key challenges in an IoV context is ensuring the computing service continuity as the vehicles move away from their serving MEH. This requires implementing an online policy to decide whether to move the entity executing the service on a MEH that is closer to the user, or to complete the computation where it started. In the former case, the user spends less energy to communicate with the MEH, but resources are spent by the network due to the migration process, both in terms of energy and time. As for the latter, standard network procedures [7] ensure that the user remains connected to the serving MEH, thus guaranteeing the delivery of the computation result, at the cost of a higher latency.

Article contribution. We propose EASE, a *proactive* approach to select the most suitable allocation of computing resources considering energy, memory and computation constraints. In the envisioned scenario, eNBs (MEHs) are connected to the power grid and empowered with photovoltaic panels (PVs), which provide green energy that can be exploited without

additional costs. Vehicle mobility predictions are leveraged to estimate the best sites where the users' computing jobs can be allocated, accounting for network and users requirements. To the best of our knowledge, this is the first attempt to designing a complete framework for the *energy efficient* scheduling of computing jobs over MEHs networks, by exploiting mobility aware procedures. The devised system provides job schedules for time slots of fixed duration, minimizing the carbon footprint at the network side – for the computation and communication services – subject to job latency and mobility constraints. The proposed job scheduling policy consists of two phases, the former is independently and locally executed at the eNBs (MEHs), while the latter is implemented as a decentralized consensus process. In the first phase, each MEH leverages estimates of the renewable (cost-free) energy, the computational power and the memory available within a prediction window to decide upon the optimal local amount of workload to be executed, subject to users' mobility and delay constraints. Each MEH also identifies the jobs that should be migrated to neighboring MEHs as associated with vehicles that are approaching the border of their current serving cell. The mobility predictor developed in [8] is used to determine the desired workload to transfer to each neighboring MEH. Then, in the second phase, the MEHs reach an agreement on the amount of workload to exchange to reduce the overall energy expenditure, while guaranteeing adequate QoS to the end-users. Here, a close-to-optimal integer solution for jobs migration is derived through a consensus algorithm followed by a rounding step, which use mobility predictions to make job migration decisions. The proposed solution is evaluated in a real-world scenario emulated through the “simulation of urban mobility” (SUMO) software, considering the vehicular mobility traces for the city of Cologne, and a dense city-wide deployment of 5G eNBs with MEC functionalities. Numerical results reveal that the developed allocation strategy significantly reduces the carbon footprint of the edge network, with an increasing gain over heuristic strategies when the available green energy is scarce. At the same time, it properly allocates workload to the processing units according to their specific computing power, by delivering better QoS to the users with respect to heuristic solutions and meeting delay constraints. When possible, service migrations also follow the user equipment (UE) during handovers.

The present work brings the following innovations.

- The problem of computation service continuity is solved in a holistic way, designing EASE, a complete framework for users' job scheduling and migration within the MEHs of a mobile edge network with distributed renewable energy resources. The main objective is to reduce

the carbon footprint of the edge computing network by exploiting the available renewable energy resources at the maximum extent.

- A two-step approach for job location management and migration is devised, splitting the problem into local and distributed phases. With it, MEHs take advantage of user mobility information (and forecasting) to reduce the energy expenditure of the edge network.
- For the distributed phase, a consensus strategy is designed to make migration decisions, and solved in closed form exploiting a dual ascent algorithm. Upon reaching consensus, an original strategy is put forward to obtain a close-to-optimal solution for workload and memory management at the MEHs.

The related work is analyzed in the next Section II, whereas the solution workflow is presented in Section III, where we also detail the remaining sections of the paper.

II. RELATED WORK

The resource allocation problem in a MEC scenario is extensively addressed in the literature. Among the most recent works, in [9] the authors present a job scheduler for containers management at the MEHs, aiming at reducing the network carbon footprint and its energy consumption. In [10], [11], the task offloading is optimized from a user perspective, minimizing the task completion time and the related energy expenditure. However, these approaches consider *static* users and, in turn, are not suitable for IoV scenarios, where the users – vehicles – move within the network area. In this article, we consider that jobs are generated by vehicles in an urban area, devising EASE, a scheduling algorithm to guarantee service continuity. The mobility management is a key aspect towards the effective implementation of MEC assisted IoV networks [12]. Computation service handovers entail not only the exchange of control messages, but also the migration of the data associated with the specific job under execution. The users' requests are served at a so called serving MEH through the instantiation of a virtual entity – either a virtual machine (VM) or a container – empowered with adequate memory and computing resources to satisfy the service requirements [13]. Therefore, when a computing service handover is triggered, the virtual entity must be transferred to the target MEH to allow restoring the computation from the point where the current serving MEH stopped. This poses several issues associated with the job latency constraints and the network energy migration costs. A paper addressing the latency challenge, and proposing strategies to reduce the migration time is [14]. The main focus is on *how* to migrate the virtual entity, by defining protocols to transfer

the container/VM from the current location to the target one. Machen et al. [15] propose a layered framework to migrate applications encapsulated either in VMs or containers, showing a reduction in the service downtime. The authors of [16] leverage the layered nature of the storage system to reduce the overhead in the container file system synchronization between the serving and the target MEHs. We stress that, the just mentioned approaches are *reactive*, i.e., the service migration is performed *after* the user has moved to the new MEH site. This results in an unavoidable processing delay due to the time required for the virtual entity re-instantiation at the new MEH. EASE is instead a *proactive* approach, as the virtual entity is migrated *before* the handover event occurs, thus reducing the service interruption time.

Proactive methods require the MEC orchestrator to predict the user's next point of attachment to trigger the migration process in advance. Some recent works in the literature show the effectiveness of such a strategy but (i) they fail to provide a complete framework to optimally allocate the computing jobs within the network entities while considering energy, memory and computing power constraints, and (ii) they rely on a centralized orchestrator that computes the best policy to adopt knowing the state of all the network entities. Among them, in [17], the authors exploit the vehicle velocity and its direction to decide if and where, i.e., in which target MEH, the virtual entity should be migrated to ensure service continuity. Campolo et al. [18] exploit the pre-planned vehicle's routes to proactively migrate the MEH container following the user's movements. In [19], the authors design an optimal decision policy to decide whether to migrate the virtual entity to the target MEH, or to keep the job execution on the first serving MEH. However, they consider a simple mobility model, using Markov chain based predictions, which is deemed inapt to prove the effectiveness of their solution in a real-world setup. A different approach is presented in [20], where the user's virtual entity is replicated to multiple neighboring MEHs before the handover event occurs. The authors suggest using mobility estimates to place the replicas, but leave this for future study. The last point is addressed in [8], where the authors integrate accurate mobility predictions into a VM replication strategy, towards reducing the network energy consumption. Rago et al. [21] use predictions on user locations and task requests to optimally and proactively allocate jobs on the available MEHs. In [22], the authors use mobility estimates to allocate users' jobs through a recursive procedure based on genetic algorithms with the sole objective of minimizing the latency (energy consumption is not addressed). In [23], user mobility predictions are instead used to allocate sufficient resources to each users' job, to ensure the completion of the process within the eNB coverage region. In [24],

the MEC service migration process and the physical route for the user to get to the destination are jointly optimized. The problem is solved through a multi-agent deep reinforcement learning approach to meet the job delay requirements with minimum migration cost and travel time. In [25], the authors study the problem of managing the energy coming from renewable sources to minimize the electricity drained from the power grid. However, unlike what we do with EASE in the present work, they disregard the mobility aspect. Moreover, they distribute the whole MPC solution, resulting in a high computational burden, while EASE performs a preliminary local phase, to reduce the complexity.

In the present contribution, we sharply depart from the existing literature by proposing EASE, an energy- and mobility-aware, distributed and proactive scheduling framework for computing jobs allocation and virtual entity migration, with the objective of minimizing the carbon footprint of the MEH network. This is achieved combining local policies with a decentralized consensus algorithm, thus obviating the need for an orchestrator.

III. SOLUTION WORKFLOW

The optimization objective of EASE amounts to minimizing the energy drained from the power grid – considering as cost free the energy that each MEH collects from renewable energy resources – while meeting memory, processing constraints and accounting for the user mobility process. A high level diagram of EASE is presented in Fig. 1. The scheduler operates according to two optimization phases: 1) local phase (left of the diagram): a predictive control phase, performed locally at each MEH node, and 2) distributed phase (right): a collaborative optimization based on distributed consensus (solved via message passing). In phase 1, the MEHs locally control the ongoing computations, estimating the local processing capacity and energy availability within a given prediction horizon. At the same time, the local algorithm assesses the amount of workload that should be migrated (“desired workload migration estimation”) to the neighboring MEH nodes, predicts insufficient local resources (“MEH resource estimation”), and accounts for mobility estimates (“next MEH prediction”), i.e., the vehicle that generated the job request is about to hand over to a neighboring radio cell.

With phase 2, taking the desired workload to be migrated from phase 1 as input (“neighbors’ resource information”), the MEHs collectively reach an agreement (“workload migration agreement”) about *how many* and *which* jobs are to be actually migrated, as well as about the target MEH for their migration (“job selection and migration”).

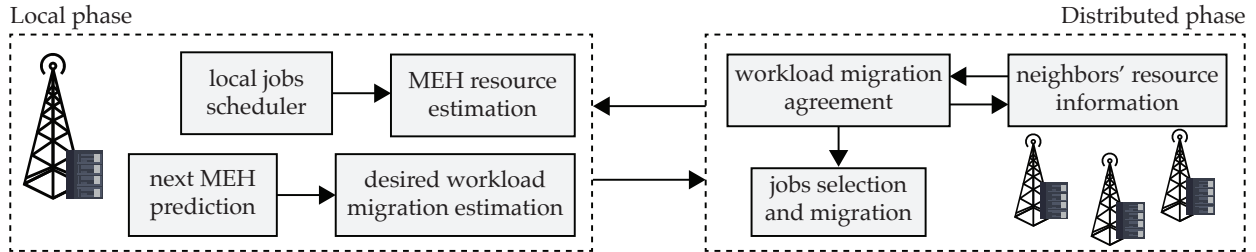


Fig. 1: **High level diagram of EASE.** The local steps are detailed on the left and provide the resource and the desired workload migration estimates for each MEH in isolation. The distributed algorithm on the right allows the MEH to reach a consensus on the jobs allocation and trigger their migration.

After step 2), each node updates its local state equations with the new jobs generated by the vehicles under coverage and those received from the neighbors, and goes back to step 1).

The remainder of this paper is organized as follows. The system model is presented in the next Section IV. A first problem formulation for the optimal scheduling is detailed in Section V. The final scheduling solution, composed of the two phases (local and distributed) is presented in Section VI. The performance assessment is reported in Section VII and final remarks are provided in Section VIII.

IV. SYSTEM MODEL

Time t is discrete and evolves according to slots of fixed duration τ , i.e., $t = 0, \tau, 2\tau, \dots$. The considered setup consists of an urban environment covered by a set \mathcal{N} of eNBs, each co-located with a MEH. \mathcal{V} represents the set of vehicles moving within the city, which are constantly connected to the nearest eNB node (providing communication support). Vehicle $v \in \mathcal{V}$ sends computing job requests to the closest MEH, which can locally execute the required workload or offload it, either partially or in full, to neighboring MEHs. Also, each vehicle can have a single outstanding job instance (being processed) and can generate a single job request at any time slot only if the previous request has been either fully processed or dropped by the serving MEH. For this reason, in the following analysis we will interchangeably identify a vehicle with the associated outstanding job to be computed. The set of neighboring eNBs to eNB i is denoted by \mathcal{N}_i . Jobs are executed through the instantiation of containers, which reserve the needed computing and memory resources. In this work, containers are favoured over VMs due to their lower memory footprint, which permits a faster migration process – a desirable feature in the considered mobile scenario [14]. Jobs that are being executed on one MEH but associated

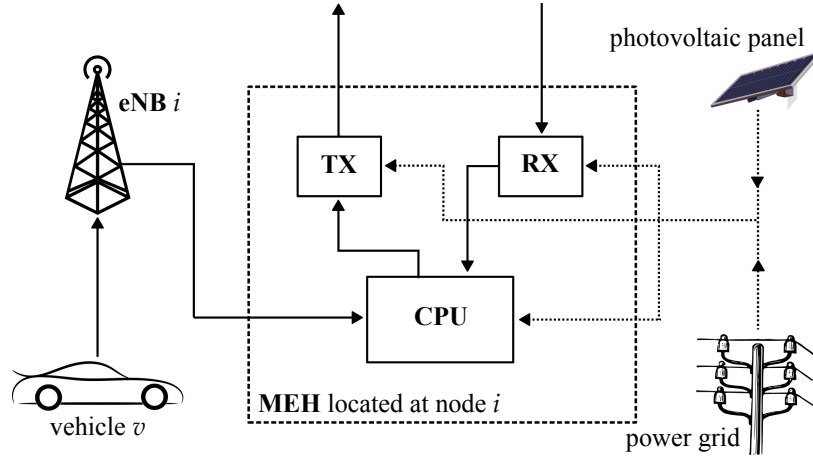


Fig. 2: **eNB/MEH node**. Job requests arrive from connected vehicles v moving within the eNB coverage area. Containers handling the execution of the jobs are created at the serving MEH, and possibly migrated to other MEHs in case the associated vehicles exit the eNB coverage area.

with vehicles that are about to leave the eNB/MEH coverage area are assessed by the migration controller. The latter decides whether to migrate their execution to another (target) MEH, or to finish it locally and send the processing result to the vehicle in a multi-hop fashion (from the old to the new serving eNB). eNBs are equipped with energy harvesting devices, e.g., PVs, whose collected energy is managed by the system. Besides, eNBs are also connected to the power grid as relying only upon harvested energy would be risky due to its intermittent nature. The diagram of an eNB/MEH node is shown in Fig. 2.

Next, we detail the mathematical models for computing and communication services, along with the statistical processes involved in the envisioned scenario and the system constraints. The mathematical notation is summarized in Table I.

A. Computation and communication models

Computing job parameters. At time t , each job k served by MEH i is characterized by the triplet $(I_{i,k}(t), D_{i,k}(t), S_{i,k}(t))$, where i) $I_{i,k}(t)$ is the residual job intensity, expressed in CPU cycles, ii) $D_{i,k}(t)$ is the residual (hard) execution deadline, in seconds, i.e., the time still available to execute the job, and iii) $S_{i,k}(t)$ is the remaining data to be processed, in bits. As the job is processed by the server, the intensity, deadline and data size decrease in accordance with the

Symbol	Meaning	Unit
$v \in \mathcal{V}$	vehicle identifier (ID) and set of vehicles	-
$i \in \mathcal{N}$	eNB/MEH ID and set of eNBs/MEHs	-
\mathcal{N}_i and N_i	set of neighboring nodes of node i and its cardinality $ \mathcal{N}_i $	-
$k \in \mathcal{K}_i(t)$ and $K_i(t)$	job ID, set of jobs in execution at MEH i at slot t , and its cardinality $ \mathcal{K}_i(t) $	-
$\hat{\mathcal{K}}_{ij}$ and \hat{K}_{ij}	set of jobs running on MEH i with probable next MEH j and its cardinality	-
T	no. of slots in the prediction horizon	-
$t = [0, \dots, T]$	scheduling time slot index	-
τ	length of a scheduling slot	s
$V_i(t)$ and $C_i(t)$	no. of results to be sent in the coverage area of eNB i at slot t and to be routed through the backhaul network	-
I_k	intensity of job k	cyc.
D_k	deadline of job k	s
S_k	size of job k	bit
p_v and p_ℓ	job generation probability and probability that it is of type ℓ	-
$\mathbf{p}_{i,k}(t)$	handover prob vector for vehicle v (job k) at slot t	-
$w_{i,k}(t)$	workload of job k processed by MEH i in slot t	cyc.
L	(fixed) size of a container instantiated on a MEH	bit
E_b^{RAN}	energy per bit for eNB-vehicle wireless transmissions	J/bit
E_b^{wired}	energy per bit for eNB-eNB wired transmission	J/bit
σ_s and σ_d	energy per bit for migration at the source (destination) MEH	J
E_s and E_d	(fixed) energy for migration at the source (destination) MEH	J
$E_i^{\text{H}}(t)$	harvested energy available at slot t	J
$P_i^{\text{PV}}(t)$	power supplied by the PV at node i , instant t	W
P_{i}^{RAN} and P_{i}^{wired}	(fixed) power to keep the wireless (wired) unit switched on	W
P_i^{idle}	(fixed) power to keep the server switched on	W
$N_i^{\text{inc}}(t)$ and $N_i^{\text{out}}(t)$	no. of MEH incoming (outgoing) jobs at slot t	-
F_i	maximum computational power of server i	W
M_i	maximum amount of RAM available at server i	bit
\bar{w}_{ij}	desired intensity requested by MEH i to neighbor j	cyc./s
\bar{m}_{ij}	memory space requested by MEH i to neighbor j	bit
\hat{P}_i^{H}	residual green power at node i after the local scheduling	W
\hat{F}_i	residual computing power at node i after local scheduling	W
\hat{M}_i	residual RAM memory at node i after the local scheduling	bit
o_{ij}	optimal amount of MEH i processing load to offload to j	cyc./s
\tilde{o}_{ji}	optimal processing load to be received at MEH i from j	cyc./s

TABLE I: Summary of the symbols used within the paper. ‘‘cyc.’’ stands for ‘‘CPU cycles’’.

following state equations

$$I_{i,k}(t + \tau) = I_{i,k}(t) - w_{i,k}(t), \quad (1)$$

$$D_{i,k}(t + \tau) = D_{i,k}(t) - \tau, \quad (2)$$

$$S_{i,k}(t + \tau) = S_{i,k}(t) - \frac{S_{i,k}(0)}{I_{i,k}(0)} w_{i,k}(t), \quad (3)$$

where $w_{i,k}(t)$ is the amount of workload belonging to job k and processed by MEH i during slot t . Note that (1) makes it possible to rewrite (3) as

$$S_{i,k}(t) = \frac{S_{i,k}(0)}{I_{i,k}(0)} I_{i,k}(t), \quad (4)$$

where the factor $S_{i,k}(0)/I_{i,k}(0)$ regulates the linear correlation between the remaining job intensity $I_{i,k}(t)$ and the data that still has to be processed for job k , $S_{i,k}(t)$.

Communication models. For the 5G wireless links between the eNBs and the vehicles we adopt i) the massive-MIMO energy consumption model of [26], and ii) the mm-wave – 28 GHz – urban NLoS channel model of [27]. Specifically, from [26] the following system parameters are obtained: i) the power needed to keep the wireless unit switched on (fixed circuit power consumption), P_{RAN} , ii) the energy required per transmitted bit via wireless links, E_b^{RAN} , iii) the fixed wired circuit power consumption, P_{wired} , iv) the energy expenditure for the wired backhaul links connecting the eNBs, E_b^{wired} . Note that the vehicles' energy utilization is not involved in the scheduling and, in turn, only the energy consumption at the eNB side is considered. The model in [27] is used for the vehicle-eNB association.

Container migration model. The migration of a container requires the hosting MEH to spend energy for freezing the status of the virtual entity and prepare the data to be sent to the target MEH for the correct re-instantiation. Hence, the target MEH has to spend energy to create the new virtual entity using the received information. The energy expenditure at the two sides consists of [28]: i) a contribution proportional to the size of the migration data, through the parameters σ_s and σ_d respectively, plus ii) a fixed energy contribution, equal to E_s for the source MEH and E_d for the target one, respectively. Additionally, the source spends some energy for transmitting the data over the wired channel E_b^{wired} . Overall, it holds

$$E_{\text{source}}^{\text{migr}}(t) = \sigma_s L + E_b^{\text{wired}} S_k(t) + E_s, \quad \text{and} \quad (5)$$

$$E_{\text{dest}}^{\text{migr}}(t) = \sigma_d L + E_d, \quad (6)$$

where $S_k(t)$ is the (variable) data size associated with job k , and L is the (fixed) container size. According to [18], we account for a service downtime of T_k^{migr} when migrating the entities. In turn, T_k^{migr} seconds are additionally removed from the job's deadline $D_k(t)$ at every migration occurrence. Note that the delay associated with wired transmissions is negligible as compared to the service downtime.

B. Statistical processes

Energy harvesting model. We refer to $P_i^{\text{PV}}(t)$ as the power supplied by the PV co-located with eNB/MEH i at instant t and that varies from a minimum of $P_{\text{min}}^{\text{PV}}$ to a maximum of $P_{\text{max}}^{\text{PV}}$.

Accounting for the power required to keep the server (P_i^{idle}) and the communication channels (P_{RAN} and P_{wired}) switched on, and the fixed amount of energy required for the container migration, the harvested energy available at eNB/MEH i for computations and data transmissions at time slot t is

$$E_i^{\text{H}}(t) = (P_i^{\text{PV}}(t) - P_{\text{RAN}} - P_{\text{wired}} - P_i^{\text{idle}}) \tau - N_i^{\text{inc}}(t) (\sigma_d L + E_d) + \quad (7)$$

$$- N_i^{\text{out}}(t) [(\sigma_s + E_b^{\text{wired}}) L + E_s]$$

where $N_i^{\text{inc}}(t)$ and $N_i^{\text{out}}(t)$ are the known number of MEH incoming and outgoing jobs at MEH i and time t , which are scheduled at the previous step $t - \tau$. The terms in Eqs. (5)-(6) that depend on the data size $S_{i,k}(t)$ are not considered in $E_i^{\text{H}}(t)$ as they will be integrated in the optimization function (see Eq. (18)). Note that being $E_i^{\text{H}}(t)$ a difference between the harvested energy and that required to deliver the services, its value can be negative. $E_i^{\text{H}}(t)$ is known for the current slot t only. However, the developed MPC framework also needs estimates for $[E_i^{\text{H}}(t + \tau), \dots, E_i^{\text{H}}(t + \tau(T - 1))]$, within the time window $t + \tau, \dots, t + \tau(T - 1)$, where T is the prediction horizon. These estimates are computed by forecasting the time dependent quantities in (7): future values of $P_i^{\text{PV}}(t + \cdot)$ are estimated using a Gaussian r.v. with average P_{PV} and standard deviation σ_{PV} , estimates for the number of incoming $N_i^{\text{inc}}(t + \cdot)$ and outgoing $N_i^{\text{out}}(t + \cdot)$ jobs at eNB i in slot t are obtained considering the vehicles in the external annulus of the eNB's coverage area. Finally, P_i^{idle} depends on the specific MEH characteristics at eNB i , as specified in Section VII.

Jobs types and arrival model. Three types of jobs are considered in this work, having different intensities, deadlines, and data sizes and identified through the index $\ell = \{1, 2, 3\}$. Every job type is associated with a generation triplet (I^ℓ, D^ℓ, S^ℓ) , and a generation probability p_ℓ . Each vehicle $v \in \mathcal{V}$ can submit at most one computing job at a time to the network facilities, so that a bijective mapping vehicle-job ID can be derived. Once a job is finished or expired, the vehicle submits a new job to the MEH with probability p_v at each slot. This parameter is tuned in the simulations. Also in this case, for predictive optimization, an estimate for the future incoming jobs is needed. To this purpose, a circular buffer containing the values of $I_{i,k}/D_{i,k}$ of the newly generated jobs is kept. A fixed estimate of the average of the last W seconds is used to predict the incoming traffic. In [25], the authors verified that even simple predictors are still effective with MPC if T is large enough.

Handover probabilities. Each job k is associated with a probability vector that depends on the

position of the vehicle v requesting the service. Being i the serving eNB for vehicle v , we define $\mathbf{p}_{i,k}(t)$ as the N_i -dimensional vector containing the probabilities that vehicle v will hand over to any of the $|\mathcal{N}_i| = N_i$ neighboring radio cells, i.e., $\mathbf{p}_{i,k}(t) = [p_{i1,k}(t), p_{i2,k}(t), \dots, p_{iN_i,k}(t)]$, with $\sum_j p_{ij,k} = 1$. Vector $\mathbf{p}_{i,k}(t)$ is updated every time a new trajectory sample is available for the associated vehicle v , either inside the same cell or in a new cell after performing the handover.

C. System constraints

The set $\mathcal{K}_i(t)$, with cardinality $K_i(t) = |\mathcal{K}_i(t)|$, collects the jobs being executed at time slot t at MEH i . The following systems constraints apply

Processing capacity. Indicating with F_i the maximum computing power of server i – expressed in CPU cycles per second – the following inequality on the sum of the workloads holds

$$\frac{1}{\tau} \sum_{k=1}^{K_i(t)} w_{i,k}(t) \leq F_i. \quad (8)$$

Storage capacity. Being M_i [bits] the maximum amount of RAM available at server i , the sum of the data sizes $S_{i,k}(t)$ of all the active jobs at MEH i must obey

$$\sum_{k=1}^{K_i(t)} S_{i,k}(t) \leq M_i. \quad (9)$$

Job execution time. In case the deadline of job k , $D_{i,k}(t)$, expires in the current time slot t , the job must be processed entirely and immediately at server i and cannot be further migrated, i.e.,

$$w_{i,k}(t) = I_{i,k}(t) \quad \text{if } D_{i,k}(t) \leq \tau. \quad (10)$$

This guarantees the timely delivery of the computation result to the requesting vehicle, avoiding that the outcome becomes useless. As Eqs. (8)-(10) may not be jointly satisfied, in the following we will relax Eq. (8).

Workload conservation. Finally, note that, in general, the inequalities

$$0 \leq w_{i,k}(t) \leq I_{i,k}(t), \quad \forall i \in \mathcal{N}, \quad \forall k \in \mathcal{K}_i(t), \quad \forall t \quad (11)$$

must always hold, because of the workload conservation principle.

V. PROBLEM FORMULATION

A. Step 1: Local controller and resources estimation

Each MEH $i \in \mathcal{N}$ estimates $w_{i,k}(t)$ for every job $k \in \mathcal{K}_i(t)$ to be executed at time t : in the analysis, $w_{i,k}(t)$ stands for the optimal fraction of computing intensity $I_{i,k}(t)$ to be locally executed at time slot t for the hosted job k . We define vectors $\mathbf{w}_i(t)$, $\mathbf{I}_i(t)$ and $\mathbf{D}_i(t)$ respectively collecting $w_{i,k}(t)$, $I_{i,k}(t)$ and $D_{i,k}(t)$ for all $k \in \mathcal{K}_i(t)$. As for the energy spent to transmit the processing results back to the vehicles, $V_i(t) E_b^{\text{RAN}}$ is the (per bit) energy cost of sending the results to the $V_i(t)$ vehicles in the wireless coverage area, while $C_i(t) E_b^{\text{wired}}$ is the energy cost entailed in routing the $C_i(t)$ jobs that are completed at node i and that have to be routed via the backhaul links to reach the corresponding user (vehicle). R_k is the size of the processing result of job k , and q_i^{proc} is the energy cost of processing a unit of workload.

Given these quantities, we define two local (at node i) functions $f_i(\cdot)$ and $g_i(\cdot)$, as follows.

$$f_i(\mathbf{w}_i; V_i, C_i, E_{\text{H},i}) = q_i^{\text{proc}} \mathbf{1}^T \mathbf{w}_i(t) + V_i(t) E_b^{\text{RAN}} R_k + C_i(t) E_b^{\text{wired}} R_k - E_i^{\text{H}}(t), \quad (12)$$

$$g_i(\mathbf{I}_i(t); \mathbf{D}_i(t)) = \sum_{k=1}^{K_i(t)} \left(\frac{I_{i,k}(t)}{D_{i,k}(t)} \right)^2. \quad (13)$$

$f_i(\cdot)$ quantifies the difference between the total energy expenditure at node i in slot t (due to processing and communications processes) and the energy that is locally harvested at this node. Hence, $-f(\mathbf{w}_i; \cdot)$ represents the residual cost-free energy available for the migration process in the distributed phase. Minimizing $f_i(\cdot)$ corresponds to maximizing the local energy available at the node. $g_i(\cdot)$ represents the residual processing cost, which is proportional to $(I_{i,k}/D_{i,k})^2$. Minimizing $g_i(\cdot)$ forces the node to execute the jobs, especially prioritizing those with high intensity and whose deadline is about to expire. Note also that, due to Eq. (1), $I_{i,k}(t)$ depends on the optimization variable $w_{i,k}$ at previous time slots.

Considering a forecast optimization window of T slots into the future, and letting $t = 0$ be the current time slot, the local cost function at node i over the whole time horizon is formulated by combining $f_i(\cdot)$ and $g_i(\cdot)$, as

$$J_i(\mathcal{W}_i, \mathcal{I}_i; \mathcal{D}_i, \mathbf{V}_i, \mathbf{C}_i, \mathbf{E}_i^{\text{H}}) = \gamma \sum_{t=0}^{T-1} g_i(\mathbf{I}_i(t); \mathbf{D}_i(t)) + \sum_{t=0}^{T-1} \max\{f_i(\mathbf{w}_i; \cdot), 0\}^2, \quad (14)$$

where \mathcal{W}_i , \mathcal{I}_i and \mathcal{D}_i represent the stacks of vectors $\mathbf{w}_i(t)$, $\mathbf{I}_i(t)$ and $\mathbf{D}_i(t)$ over the considered

horizon T , respectively, while \mathbf{V}_i , \mathbf{C}_i and \mathbf{E}_i^H are the vectors collecting $V_i(t)$, $C_i(t)$ and $E_i^H(t)$ for $t \in \{0, \tau, \dots, \tau(T-1)\}$. The coefficient $\gamma > 0$ is used to balance the processing state cost term ($g_i(\cdot)$) with respect to the energy cost ($f_i(\cdot)$).

Remark 1. From a physical perspective, the processing energy consumption is not necessarily a quadratic function, but it varies based on the specific computing architecture [29]. A quadratic function for $f_i(\cdot)$ was chosen, as it promotes smoothness of the controller in the transitions from a slot to the next one, and has the same curvature order of the processing state cost $g_i(\cdot)$. Also, the $\max\{\cdot\}$ function is used to make the cost positive only when $f_i(\cdot) > 0$, i.e., the renewable energy is fully used and the node has to resort to the power grid.

Next, the cost function in Eq. (14) is modified through the addition of a penalty term proportional to two new auxiliary variables $\boldsymbol{\delta}_i(t) = [\delta_{F_i}(t), \delta_{M_i}(t)]$, to ensure that the problem does not become infeasible when resources are scarce. Therefore, rewriting the constraints (8) and (9), we define for each MEH the following local problem at node i ,

$$\begin{aligned}
 P_i^{\text{loc}} : \quad & \min_{\mathcal{W}_i, \boldsymbol{\delta}_i} J_i(\mathcal{W}_i, \boldsymbol{\delta}_i; \cdot) + c_i \sum_{t=0}^{T-1} \boldsymbol{\delta}_i(t) \\
 \text{s.t.} \quad & (1)-(3), (10), (11), \\
 & \frac{1}{\tau} \sum_{k \in \mathcal{K}_i} w_{i,k}(t) - \delta_{F_i}(t) \leq F_i, \\
 & \sum_{k \in \mathcal{K}_i} S_{i,k}(t) - \delta_{M_i}(t) \leq M_i,
 \end{aligned} \tag{15}$$

where $c_i > 0$ is the coefficient weighting the penalty variables. By solving (15), each MEH obtains the optimal control $\mathbf{w}_i(0)$ which is implemented in the current time step.

B. Step 2: workload migration

From (15), each server estimates its own future energy and processing resources. Specifically, let \hat{P}_i^H be the residual available green power, possibly negative if the grid support is sought, \hat{F}_i , and \hat{M}_i be the residual computational power, and RAM memory at node i , respectively. Note that, since constraints (8) and (9) are relaxed in (15), \hat{F}_i and \hat{M}_i can be negative. These estimates are obtained averaging the values over the prediction horizon, excluding the current instant $t = 0$. Due to this averaging operation, while in (15) we deal with energy expenditures, in the following we refer to power quantities.

The migration task presents itself as a combinatorial mixed integer programming (MIP) problem, which is non-convex and is generally difficult to solve in a distributed fashion. Thus, we use heuristics to derive close-to-optimal solutions. In this work, the popular *relax and round* method is used, which consists in solving the convex counterpart of the original problem, and rounding the result to a feasible solution afterwards.

Based on the handover probability vector $\mathbf{p}_{i,k}$ presented in Section IV-B, each MEH determines the average resource demand requested from its neighbors in the migration process. Specifically, the CPU cycles per second and memory space that are requested from neighbor j are

$$\bar{w}_{ij} = \sum_{k \in \hat{\mathcal{K}}_{ij}} \frac{I_{i,k}}{D_{i,k}}, \quad \text{and} \quad (16)$$

$$\bar{m}_{ij} = \sum_{k \in \hat{\mathcal{K}}_{ij}} S_{i,k}, \quad (17)$$

respectively, where $\hat{\mathcal{K}}_{ij}$ represents the set of jobs that are currently running at server i , associated with vehicles that are about to exit the coverage area of the co-located eNB i and whose most probable next eNB is co-located with MEH j . With $\bar{\mathbf{w}}_i = [\bar{w}_{i1}, \dots, \bar{w}_{iN_i}]$ we denote the vector collecting the *desired* processing intensity per second to be sent to each of the N_i neighbors of MEH i , computed via (16). We also introduce the new optimization variables $\mathbf{o}_i = [o_{i1}, \dots, o_{iN_i}]$ and $\tilde{\mathbf{o}}_i = [\tilde{o}_{1i}, \dots, \tilde{o}_{N_i i}]$ representing the optimal total amount of processing load to be sent to, and to be received from each neighbor, respectively. The deviation from the desired $\bar{\mathbf{w}}_i$ to be migrated is penalized with the l_2 -norm $\|\bar{\mathbf{w}}_i - \mathbf{o}_i\|^2$, and the migration cost is defined as

$$\Gamma_i \left(\mathbf{o}_i, \tilde{\mathbf{o}}_i; \bar{\mathbf{w}}_i, \hat{P}_i^{\text{H}} \right) = \max \left\{ (q_i^{\text{tx}} - q_i^{\text{proc}}) \mathbf{1}^T \mathbf{o}_i + (q_i^{\text{rx}} + q_i^{\text{proc}}) \mathbf{1}^T \tilde{\mathbf{o}}_i - \hat{P}_i^{\text{H}}, 0 \right\} + \rho \|\mathbf{o}_i - \bar{\mathbf{w}}_i\|^2, \quad (18)$$

where q_i^{proc} , q_i^{tx} and q_i^{rx} are the processing, transmission and reception costs of server i (expressed as powers), respectively. The $\max\{\cdot\}$ term represents the power needed from the power grid to migrate the jobs, whereas the quadratic term encodes the fact that the optimal \mathbf{o}_i should be as close as possible to the desired $\bar{\mathbf{w}}_i$ – this corresponds to moving the jobs to the next serving eNB. Finally, $\rho > 0$ is a weight that balances the importance of the two cost terms. Note that minimizing Eq. (18) returns a solution \mathbf{o}_i that matches vector $\bar{\mathbf{w}}_i$ if the residual harvested power is sufficient and the constraints are satisfied. Specifically, as system constraint we consider the

following variation of (8) and (9),

$$\sum_{j \in \mathcal{N}_i} (\tilde{o}_{ji} - o_{ij}) \leq \min\{\hat{F}_i, \xi_{M_i} \hat{M}_i\} + \hat{\delta}_i, \quad \forall i \in \mathcal{N}. \quad (19)$$

Remark 2. The meaning of this constraint is that the workload surplus that server i has during the following time steps, i.e., the *incoming* workload minus the *outgoing* one, should satisfy the average (long-term) power (\hat{F}_i) and memory (\hat{M}_i) availability at node i . The coefficient ξ_{M_i} relates the memory availability to the residual computational power. This follows from the assumption of direct proportionality between the data size S_k and the processed workload w_k .

Since the general goal is to minimize the energy drained network-wide from the power grid, a cost function that represents the global welfare and at that at the same time is amenable to a distributed solution is the sum

$$\Gamma(\mathbf{o}, \tilde{\mathbf{o}}, \hat{\boldsymbol{\delta}}; \bar{\mathbf{w}}, \hat{\mathbf{P}}^H) = \sum_{i \in \mathcal{N}} \left[\Gamma_i(\mathbf{o}_i, \tilde{\mathbf{o}}_i; \bar{\mathbf{w}}_i, \hat{P}_i^H) + \hat{c}_i \hat{\delta}_i^2 \right], \quad (20)$$

where $\hat{c}_i > 0$ is the cost coefficient associated with the penalty term $\hat{\delta}_i^2$. This leads to the constrained optimization problem

$$\begin{aligned} P^{\text{glob}} : \quad & \min_{\mathbf{o}, \tilde{\mathbf{o}}, \hat{\boldsymbol{\delta}}} \Gamma(\mathbf{o}, \tilde{\mathbf{o}}, \hat{\boldsymbol{\delta}}; \bar{\mathbf{w}}, \hat{\mathbf{P}}^H) \\ & \text{s.t.} \quad \mathbf{o}, \tilde{\mathbf{o}}, \hat{\boldsymbol{\delta}} \geq 0, \quad (19), \\ & \quad \quad o_{ij} = \tilde{o}_{ij} \quad \forall i, j, \end{aligned} \quad (21)$$

with \mathbf{o} , $\tilde{\mathbf{o}}$, $\hat{\boldsymbol{\delta}}$, $\bar{\mathbf{w}}$ and $\hat{\mathbf{P}}^H$ being the vectors collecting \mathbf{o}_i , $\tilde{\mathbf{o}}_i$, $\hat{\delta}_i$, $\bar{\mathbf{w}}_i$ and \hat{P}_i^H respectively, for all the MEHs $i \in \mathcal{N}$. The equality $o_{ij} = \tilde{o}_{ij}$ is called *consensus constraint* and is added to ensure that the amount of workload exiting node i and directed to j is equal to the one that j expects to receive from i .

VI. FINAL SCHEDULING SOLUTION VIA LOCAL AND DISTRIBUTED PROCESSES

A. Step 1: local MPC solution

At each MEH, the local MPC problem of (15) is solved over the whole horizon T [30]. MPC uses the *receding horizon* technique, which consists of solving the given problem within a prediction window of size T , applying the optimal computed control only for the current time step $t = 0$, moving forward the optimization window by one time slot (τ seconds) and repeating

the procedure. In this way, the controller progressively adapts to new observations and estimates of the exogenous processes. In the considered setup, at any given instant, MEH i computes the optimal policy throughout the whole horizon of T slots, but only $\mathbf{w}_i(0)$ is applied as the control action. The exogenous processes are the future jobs and the harvested energy availability, see Section IV-B.

B. Step 2a: distributed workload migration

In the following, the scheduling slot index t is omitted in the interest of readability. Eq. (21) is a *consensus* problem, i.e., it entails the reaching of an agreement on the value of some variables among multiple agents in a distributed system. In our context, the MEHs must agree on the amount of processing load to exchange among each other. A way to solve this problem – written as the sum of separable convex cost functions – is via the *dual ascent* algorithm [31]. Given a generic cost function $\psi(\mathbf{x})$, its *Lagrangian* is defined as

$$\mathcal{L}(\mathbf{x}, \mathbf{z}) = \psi(\mathbf{x}) + \mathbf{z}^T(A\mathbf{x} - \mathbf{d}), \quad (22)$$

where \mathbf{z} are the Lagrange multipliers associated with the constraints $A\mathbf{x} = \mathbf{d}$. The dual ascent solves the problem by iteratively i) minimizing $\mathcal{L}(\mathbf{x}, \mathbf{z})$ with respect to \mathbf{x} (primal step), and ii) updating the value of \mathbf{z} (dual step). To formalize the solution of problem (21) via dual ascent, we split the local cost functions (18) as

$$\begin{aligned} \tilde{\Gamma}_i(\mathbf{o}_i, \tilde{\mathbf{o}}_i, \hat{\delta}) = & \max \left\{ (q_i^{\text{tx}} - q_i^{\text{proc}}) \mathbf{1}^T \mathbf{o}_i + (q_i^{\text{rx}} + q_i^{\text{proc}}) \mathbf{1}^T \tilde{\mathbf{o}}_i - \hat{P}_i^{\text{H}}, 0 \right\} + \\ & + \frac{\rho}{2} \|\mathbf{o}_i - \bar{\mathbf{w}}_i\|^2 + \frac{\rho}{2} \|\tilde{\mathbf{o}}_i - \tilde{\mathbf{w}}_i\|^2 + \hat{c}_i \hat{\delta}_i^2, \end{aligned} \quad (23)$$

exploiting the fact that $o_{ij} = \tilde{o}_{ij}$, and defining $\tilde{\mathbf{w}}_i = \{\bar{w}_{ji} \mid j \in \mathcal{N}_i\}$. Intuitively, node i is responsible for half of the quadratic cost from its neighbors and for half of its own local cost. For compactness, let $\mathbf{x} = \{\mathbf{x}_i = [\mathbf{o}_i, \tilde{\mathbf{o}}_i, \hat{\delta}_i], \forall i \in \mathcal{N}\}$ be the global optimization variable, $\mathbf{b}_i = [\bar{\mathbf{w}}_i, \tilde{\mathbf{w}}_i, 0]$ the tracking target vector, and $\mathbf{q}_i = [q_i^{\text{tx}} - q_i^{\text{proc}}, q_i^{\text{rx}} + q_i^{\text{proc}}, 0]$ the linear costs vector. Moreover, we define matrix $Q_i = I_{2N_i+1} \mathbf{m}_i$, with $\mathbf{m}_i = [\frac{\rho}{2}, \dots, \frac{\rho}{2}, \hat{c}_i]$, and the global block diagonal matrix Q , collecting each Q_i on the diagonal. With these definitions, problem (21) can be expressed in

the following form

$$\min_{\mathbf{x}} \sum_{i \in \mathcal{N}} \left(\|\mathbf{x}_i - \mathbf{b}_i\|_{Q_i}^2 + \max \left\{ \mathbf{q}_i^T \mathbf{x}_i - \hat{P}_i^H, 0 \right\} \right) \quad (24)$$

$$\text{s.t. } A_1 \mathbf{x} \leq \mathbf{d}, \quad (25)$$

$$A_2 \mathbf{x} = \mathbf{0}, \quad (26)$$

where $\|\mathbf{x}\|_Q^2 = \mathbf{x}^T Q \mathbf{x}$. The inequalities (25) collect (19) and the non-negativity constraints $\mathbf{o}, \tilde{\mathbf{o}}, \hat{\delta} \geq 0$, while the equalities (26) correspond to the consensus constraints $o_{ij} = \tilde{o}_{ij}, \forall i \in \mathcal{N}, j \in \mathcal{N}_i$. Here, the matrices A_1 and A_2 are used to select the concerned variables, whereas $\mathbf{d} = \{\mathbf{d}_i = [\min\{\hat{F}_i, \xi_{M_i} \hat{M}_i\}, \mathbf{0}] \mid i \in \mathcal{N}\}$. We can now write the Lagrangian as

$$\mathcal{L}(\mathbf{x}, \mathbf{y}, \mathbf{z}) = \sum_{i \in \mathcal{N}} \tilde{\Gamma}_i(\mathbf{x}_i; \mathbf{b}_i, \hat{P}_i^H) + \mathbf{y}^T (A_1 \mathbf{x} - \mathbf{d}) + \mathbf{z}^T A_2 \mathbf{x}, \quad (27)$$

where $\mathbf{y} = \{\mathbf{y}_i = [\lambda_i, \gamma_i, \tilde{\gamma}_i, \hat{\varphi}_i] \mid i \in \mathcal{N}\}$ are the Lagrange multipliers associated with the inequality constraints (25), and $\mathbf{z} = \{\mathbf{z}_i = \boldsymbol{\mu}_i \mid i \in \mathcal{N}\}$ are the multipliers associated with equalities (26). Specifically, the Lagrange multipliers λ_i refer to constraints (19), $\gamma_i = \{\gamma_{ij}\}$, $\tilde{\gamma}_i = \{\tilde{\gamma}_{ji}\}$ and $\hat{\varphi}_i$ to $\mathbf{o}_i \geq 0$, $\tilde{\mathbf{o}}_i \geq 0$, and $\hat{\delta}_i \geq 0$, respectively, and $\boldsymbol{\mu}_i = \{\mu_{ij}\}$ to $o_{ij} = \tilde{o}_{ij}$, for every server $i \in \mathcal{N}$, and $j \in \mathcal{N}_i$. Using the $+$ sign to denote the update at the following iteration, we detail in Algorithm 1 the dual ascent procedure that solves the problem

$$\inf_{\mathbf{x}} \sup_{\mathbf{y} \geq 0, \mathbf{z}} \mathcal{L}(\mathbf{x}, \mathbf{y}, \mathbf{z}). \quad (28)$$

Algorithm 1 Dual ascent algorithm solving problem (21)

- | | |
|--|--------------------------------|
| 1: $\mathbf{x}^+ = \operatorname{argmin}_{\mathbf{x}} \mathcal{L}(\mathbf{x}, \mathbf{y}, \mathbf{z})$ | ▷ primal step |
| 2: $\mathbf{y}^+ = \max \{\mathbf{y} + \boldsymbol{\alpha}_y (A_1 \mathbf{x}^+ - \mathbf{d}), 0\}$ | ▷ dual update for inequalities |
| 3: $\mathbf{z}^+ = \mathbf{z} + \boldsymbol{\alpha}_z A_2 \mathbf{x}^+$ | ▷ dual update for equalities |
-

The dual update requires in this case two different forms, depending on whether the constraint is an equality or an inequality one. Inequality constraints may actually be inactive, and the associated Lagrange multipliers would be null in this case. The parameters $\boldsymbol{\alpha}_y$ and $\boldsymbol{\alpha}_z$ in the algorithm tune the stability and the convergence speed. The presented compact version of the dual ascent translates into the following local procedure, from a server perspective. Defining the vectors $\tilde{\boldsymbol{\mu}}_i = \{\mu_{ji}\}$ and $\tilde{\mathbf{o}}_i = \{\tilde{o}_{ij}\}$ collecting variables that are kept in memory by the

neighborhoods of i , the local Lagrangian at node i is

$$\begin{aligned} \mathcal{L}_i(\mathbf{o}_i, \tilde{\mathbf{o}}_i; \tilde{\mathbf{w}}_i, \tilde{\mathbf{w}}_i, \hat{P}_i^H) &= \tilde{\Gamma}_i(\mathbf{o}_i, \tilde{\mathbf{o}}_i; \tilde{\mathbf{w}}_i, \tilde{\mathbf{w}}_i, \hat{P}_i^H) + \lambda_i \left[\mathbf{1}^T (\tilde{\mathbf{o}}_i - \mathbf{o}_i) - \hat{\delta}_i \right] + \\ &\quad - \gamma_i^T \mathbf{o}_i - \tilde{\gamma}_i^T \tilde{\mathbf{o}}_i + \boldsymbol{\mu}_i^T \mathbf{o}_i - \tilde{\boldsymbol{\mu}}_i^T \tilde{\mathbf{o}}_i - \hat{\varphi}_i \hat{\delta}_i, \end{aligned} \quad (29)$$

and the procedure is presented in Algorithm 2, where a fixed step size α is assumed.

Algorithm 2 Dual ascent from a server perspective

- 1: receive $\tilde{\boldsymbol{\mu}}_i = \{\mu_{ji}\}$ from the neighbors
 - 2: $\mathbf{o}_i^+, \tilde{\mathbf{o}}_i^+, \hat{\delta}_i = \operatorname{argmin}_{\mathbf{x}_i} \mathcal{L}_i(\mathbf{x}_i, \boldsymbol{\nu}_i)$
 - 3: send \tilde{o}_{ji}^+ to the correspondent neighbor j
 - 4: $\lambda_i^+ = \max \left\{ \lambda_i + \alpha \left(\sum_{j \in \mathcal{N}_i} (\tilde{o}_{ji}^+ - o_{ij}^+) - \hat{F}_i \right), 0 \right\}$
 - 5: $\hat{\varphi}_i^+ = \max \left\{ \hat{\varphi}_i - \alpha \hat{\delta}_i^+, 0 \right\}$
 - 6: $\gamma_i^+ = \max \left\{ \gamma_i - \alpha \mathbf{o}_i^+, 0 \right\}$
 - 7: $\tilde{\gamma}_i^+ = \max \left\{ \tilde{\gamma}_i - \alpha \tilde{\mathbf{o}}_i^+, 0 \right\}$
 - 8: receive $\bar{\mathbf{o}}_i^+ = \{\tilde{o}_{ij}^+\}$ from the neighbors
 - 9: $\boldsymbol{\mu}_i^+ = \boldsymbol{\mu}_i + \alpha (\mathbf{o}_i^+ - \bar{\mathbf{o}}_i^+)$
 - 10: send μ_{ij}^+ to the correspondent neighbor j
-

Note that, to minimize the Lagrangian in the primal step at line 2, server i not only needs its own Lagrange multipliers, but also the introduced $\tilde{\boldsymbol{\mu}}_i$, which collects the μ_{ji} of neighbors $j \in \mathcal{N}_i$. Therefore, node i must first receive these multipliers from the neighborhood. Also, while updating $\boldsymbol{\mu}_i$ in the dual step at line 9, $\bar{\mathbf{o}}_i^+$ is needed, which collects the \tilde{o}_{ij}^+ variables kept by the neighborhood of i , and which are to be received after the computation of j 's primal step ($\forall j \in \mathcal{N}_i$). Hence, this amounts in two communication rounds among neighbors per dual ascent iteration. The dual updates are computationally inexpensive, whereas the primal step requires to solve a local convex subproblem, which is complicated by the $\max\{\cdot\}$ operator in the cost function (23). Eventually, note that an additional communication is required at the beginning of the procedure, to inform the neighborhood about the values of $\tilde{\mathbf{w}}_i$.

Solution to the primal step (line 2). The solution of the local primal subproblems is computed in closed form, distinguishing three cases. We consider the local primal subproblems in compact form with variables \mathbf{x}_i , and collect the Lagrange multipliers of (29) in $\boldsymbol{\nu}_i = [\lambda_i \mathbf{1}, \varphi_i, \boldsymbol{\gamma}_i, \tilde{\boldsymbol{\gamma}}_i, \boldsymbol{\mu}_i, \tilde{\boldsymbol{\mu}}_i]$,

with associated variables selection matrix A_i . We split $\mathcal{L}_i(\mathbf{x}_i; \cdot) = u_i(\mathbf{x}_i) + h_i(\mathbf{x}_i)$, so that

$$u_i(\mathbf{x}_i) = \|\mathbf{x}_i - \mathbf{b}_i\|_{Q_i}^2 + \boldsymbol{\nu}_i^T A_i \mathbf{x}_i, \quad (30)$$

$$h_i(\mathbf{x}_i) = \mathbf{q}_i^T \mathbf{x}_i - \hat{P}_i^H. \quad (31)$$

Proposition 1. *The solution of the primal step of problem (21) is computed as one of the mutually exclusive cases*

- i) $\mathbf{x}_i^+ = \operatorname{argmin}_{\mathbf{x}_i} u_i(\mathbf{x}_i)$, if $h_i(\mathbf{x}_i^+) \leq 0$, or
- ii) $\mathbf{x}_i^+ = \operatorname{argmin}_{\mathbf{x}_i} u_i(\mathbf{x}_i) + h_i(\mathbf{x}_i)$, if $h_i(\mathbf{x}_i^+) > 0$, or
- iii) $\mathbf{x}_i^+ = \operatorname{argmin}_{\mathbf{x}_i} u_i(\mathbf{x}_i)$, s.t. $h_i(\mathbf{x}_i) = 0$.

Proof: i) and ii) correspond to the cases where the $\max\{\cdot\}$ operator in (23) is replaced by 0 or $h_i(\mathbf{x}_i)$, respectively. Once the optimum is computed, the feasibility check must be done: if the minimum lies in the feasible region, the solution is accepted. However, it can also be that these two optima are both infeasible: in this case, the optimal solution must lie on the plane $h_i(\mathbf{x}_i) = 0$, and a constrained problem has to be solved (case iii). ■

Remark 3. It is impossible that both solutions i) and ii) are feasible, otherwise the convex function (23) would have two minima, which is an absurd due to its convexity.

The solutions for each of the cases of Proposition 1 are now given in the following result.

Proposition 2. *Consider the three cases of Proposition 1. Their closed form optimal solutions are expressed as*

- i) $\mathbf{x}_i^+ = \mathbf{b}_i - \frac{1}{2} Q_i^{-1} A_i^T \boldsymbol{\nu}_i$
- ii) $\mathbf{x}_i^+ = \mathbf{b}_i - \frac{1}{2} Q_i^{-1} (A_i^T \boldsymbol{\nu}_i + \mathbf{q}_i)$
- iii) $\mathbf{x}_i^+ = \mathbf{b}_i - \frac{1}{2} Q_i^{-1} \left(A_i^T \boldsymbol{\nu}_i + \mathbf{q}_i^T \frac{2 Q_i \left(\mathbf{b}_i - \frac{\hat{P}_i^H}{\|\mathbf{q}_i\|^2} \mathbf{q}_i \right) - A_i^T \boldsymbol{\nu}_i}{\|\mathbf{q}_i\|^2} \mathbf{q}_i \right)$

Proof: The proof is straightforward for cases i) and ii): it is sufficient to set the gradient of the function to zero. In the third case, it is necessary to solve the constrained minimization of $u(\mathbf{x}_i)$ subject to $h(\mathbf{x}_i) = 0$. The Lagrange multipliers method can be used, where the Lagrangian of case iii) is $\mathcal{L}'(\mathbf{x}_i, \eta_i) = u(\mathbf{x}_i) + \eta_i h(\mathbf{x}_i)$, and its primal solution is

$$\inf_{\mathbf{x}_i} \sup_{\eta_i} \|\mathbf{x}_i - \mathbf{b}_i\|_{Q_i}^2 + \boldsymbol{\nu}_i^T A_i \mathbf{x}_i + \eta_i \left(\mathbf{q}_i^T \mathbf{x}_i - \hat{P}_i^H \right). \quad (32)$$

The partial derivatives with respect to \mathbf{x}_i , and η_i are

$$\frac{\partial \mathcal{L}'(\mathbf{x}_i, \eta_i)}{\partial \mathbf{x}_i} = 2 Q_i (\mathbf{x}_i - \mathbf{b}_i) + A_i^T \boldsymbol{\nu}_i + \eta_i \mathbf{q}_i, \quad (33)$$

$$\frac{\partial \mathcal{L}'(\mathbf{x}_i, \eta_i)}{\partial \eta_i} = \mathbf{q}_i^T \mathbf{x}_i - \hat{P}_i^H. \quad (34)$$

Setting them to zero, we obtain

$$\mathbf{x}_i = \mathbf{b}_i - \frac{1}{2} [Q_i^{-1} (A_i^T \boldsymbol{\nu}_i + \eta_i \mathbf{q}_i)] = \frac{\hat{P}_i^H}{\|\mathbf{q}_i\|^2} \mathbf{q}_i, \quad (35)$$

from which it is possible to derive the optimal value for the Lagrange multiplier

$$\eta_i^* = \frac{\mathbf{q}_i^T \left[2 Q_i \left(\mathbf{b}_i - \frac{\hat{P}_i^H}{\|\mathbf{q}_i\|^2} \mathbf{q}_i \right) - A_i^T \boldsymbol{\nu}_i \right]}{\|\mathbf{q}_i\|^2}. \quad (36)$$

Now, plugging (36) into (35) returns the optimal value \mathbf{x}_i^+ of case iii). ■

Remark 4. For quadratic programs it is also possible to find a condition on the step size α for which the algorithm is ensured to converge. This only depends on the constraint matrices A_1 and A_2 , and on the quadratic cost matrix Q defining the curvature. Since these values do not change among the three different primal optimization cases, a common condition can be obtained, i.e.,

$$\alpha \leq \frac{2}{\left\| \begin{bmatrix} A_1 \\ A_2 \end{bmatrix} Q^{-1} \begin{bmatrix} A_1 \\ A_2 \end{bmatrix}^T \right\|}. \quad (37)$$

Proof: This result can be derived using proposition 2.3.2 of [31]. ■

C. Step 2b: rounding to a feasible discrete solution

In this section, we show how to compute the actual discrete allocation of jobs by obtaining new variables \mathbf{o}_i^r , which are the *rounded* versions of the \mathbf{o}_i that were previously computed through consensus (see Section VI-B). In particular, \mathbf{o}_i contains the optimal continuous amount of workload that each MEH would like to send to its neighbors. Instead, its rounded version \mathbf{o}_i^r contains a feasible allocation accounting for the facts that the number of jobs and the possible ways of allocating them are discrete.

To compute the new \mathbf{o}_i^r , as an initial solution, we select the jobs from set $\hat{\mathcal{K}}_{ij}$, whose associated vehicle is about to migrate from eNB site i to j . The rounded \mathbf{o}_i^r is thus initially set to $\bar{\mathbf{w}}_i$,

Algorithm 3 Job-neighbor association

```

1: Input: mobility pattern predictions matrix  $P_i$ ; optimal outgoing workload amount  $\mathbf{o}_i$ ; set of
   the jobs  $\mathcal{J}_i$  in execution at MEH  $i$ ; tolerance threshold  $\epsilon_P$ .
2: Output: job-neighbor association sets  $\mathcal{Z}_{ij} \forall j \in \mathcal{N}_i$ ; rounded  $\mathbf{o}_i^r$ .
3: remove jobs  $\{k \mid I_{i,k} < \epsilon \vee D_{i,k} < 2\}$  from  $\mathcal{J}_i$ 
4:  $\mathbf{o}_i^r \leftarrow \hat{\mathbf{w}}_i$ 
5:  $\mathcal{Z}_{ij} \leftarrow \hat{\mathcal{K}}_{ij}$ 
6:  $\mathcal{J}_i \leftarrow \mathcal{J}_i \setminus \bigcup_{j \in \mathcal{N}_i} \hat{\mathcal{K}}_{ij}$ 
7:  $\mathbf{o}_i^{\text{diff}} \leftarrow \mathbf{o}_i^r - \mathbf{o}_i$  ▷ workload to be adjusted
8: for all neighbors  $j$  in  $\mathcal{N}_i$  do
9:   while  $\mathbf{o}_{ij}^{\text{diff}} > \epsilon_P$  do
10:     $k \leftarrow$  job of  $\mathcal{Z}_{ij}$  minimizing  $|\mathbf{o}_{ij}^{\text{diff}}|$ 
11:    remove job  $k$  from  $\mathcal{Z}_{ij}$ 
12:     $\mathbf{o}_{ij}^r \leftarrow \mathbf{o}_{ij}^r - I_{i,k}/D_{i,k}$ 
13:     $\mathbf{o}_{ij}^{\text{diff}} \leftarrow \mathbf{o}_{ij}^{\text{diff}} - I_{i,k}/D_{i,k}$ 
14:    add job  $k$  to  $\mathcal{J}_i$  ▷ make it available for other neighbors
15:   end while
16:   while  $\mathbf{o}_{ij}^{\text{diff}} < -\epsilon_P$  do
17:    take job  $k \in \mathcal{J}_i \mid k \in \text{argmax } \mathbf{p}_{ij}$  ▷ most probable job from  $i$  to  $j$ 
18:    add job  $k$  to  $\mathcal{Z}_{ij}$ 
19:     $\mathbf{o}_{ij}^r \leftarrow \mathbf{o}_{ij}^r + I_{i,k}/D_{i,k}$ 
20:     $\mathbf{o}_{ij}^{\text{diff}} \leftarrow \mathbf{o}_{ij}^{\text{diff}} + I_{i,k}/D_{i,k}$ 
21:    mask entry  $\mathbf{p}_{ij,k}$  ▷ s.t.  $k$  is not selected again
22:   end while
23: end for

```

assuming that the minimizer of the objective function (18) is the vector that minimizes the quadratic term. Then, the difference between this guess and the actual optimum obtained from the proposed dual ascent algorithm is computed, $\mathbf{o}_i^{\text{diff}}$. For every neighbor j it is now clear whether more workload is to be added to (in case $\mathbf{o}_{ij}^{\text{diff}} < 0$) or removed from ($\mathbf{o}_{ij}^{\text{diff}} > 0$) the initial guess \mathbf{o}_{ij}^r . The jobs that were initially scheduled for migration to node j but that are eventually retained for computation at node i are those minimizing $\|\mathbf{o}_i^{\text{diff}}\|_1$. Instead, new jobs are added to the migration list using the prediction vectors \mathbf{p}_{ij} . In detail, the added jobs are those for which the handover probabilities towards j are maximized. A threshold ϵ_P is used to approximate the rounded solution, as the continuous optimum \mathbf{o}_i will likely not coincide with any possible discrete approximation. The procedure is detailed in Algorithm 3.

D. Handling pathological cases

Since system constraints are made soft to avoid primal infeasibility, three pathological cases may occur, namely, 1) the optimal processed workload at the current instant exceeds the computational capacity; or 2) the data size for the currently running jobs do not fit the RAM memory; or 3) the deadline expires during the current slot, but the residual intensity is greater than zero. A greedy algorithm is developed to handle all of them. For the first two cases, the MEH ranks the active jobs through a double ordering criterion, considering as the first ranking criterion the time slot when they expire, and as the second their intensity (or data size). Next, it momentarily pauses the execution of the services starting from the last one in the ordered list, until the resources suffice to proceed. In case 1, when pausing a job m , the amount of processed workload becomes $\sum_{k \in \mathcal{K}_i} w_{i,k} - w_{i,m}$, while in case 2, the data relative to suspended jobs is deleted from the RAM. The number of suspended jobs is the minimum such that the requirements are satisfied. Moreover, in case 1, it is likely that, when a job is suspended, additional computational power becomes available. In such a case, the new computational resources are assigned to the jobs that are closest to their deadline. Case 3 is managed considering the amount of residual intensity $I_{i,k}$. If $I_{i,k}$ is smaller than a threshold ϵ , then the deadline is extended by a small amount, so that the controller will privilege the execution of the corresponding job in the next slot. In this way, jobs are allowed to finish with a little additional delay (within one slot). If, however, the amount of residual intensity is larger than ϵ , the job is dropped, i.e., in this case the scheduling algorithm failed to provide an acceptable solution.

VII. NUMERICAL RESULTS

The proposed job scheduling algorithm is assessed in an emulated environment featuring 5G-enabled vehicles moving within an urban scenario. Mobility traces are obtained with SUMO [32], an open-source traffic simulator that allows generating the movement of mobile users around a predefined city road map. Specifically, we use the ‘‘TAPAS Cologne’’ scenario, which mimics the vehicular traffic within the city of Cologne for a whole day on the basis of travelling habits of the city dwellers [33]. The mobile network is composed of 8 eNBs endowed with MEH functionalities, wired connected through optical links. The mobility area is covered with hexagonal cells with an eNB in the center, and with an inter-distance among nodes of 400 m. We generated and collected 24h long SUMO mobility traces with 25 ms granularity, for each of the 8 eNBs in the deployment. The first 15 hours were used to train and validate the mobility prediction

	HP ProLiant DL 110	Nettrix R620 G40
idle power P_i^{idle}	94 W	110 W
max load power P_i^{max}	299 W	468 W
computational power F_i	3.3 Gflops	7.6 Gflops
RAM memory M_i	64 GB	256 GB

	I^ℓ [Gflop]	D^ℓ [s]	S^ℓ [GB]	p_ℓ
type 1	10	20	2	0.4
type 2	16	30	10	0.2
type 3	12	40	0.1	0.4

TABLE II: Servers specifications [29].

TABLE III: Jobs parameters for the simulations.

Parameter	Value
number of nodes $ \mathcal{N} $	8
fixed wireless circuit power consumption P_{RAN}	50.2 W
fixed wired circuit power consumption P_{wired}	20 W
energy per transmitted bit via wireless link E_b^{RAN}	1 nJ/bit
energy per transmitted bit via wired link E_b^{wired}	250 pJ/bit
PV panel minimum power $P_{\text{min}}^{\text{PV}}$	250 W
PV panel maximum power $P_{\text{max}}^{\text{PV}}$	400 W
PV panel average power P_{PV}	370 W
PV panel power std σ_{PV}	10 W
containers' size L	50 MB
weight parameters for L in (6) σ_s, σ_d	500 nJ/bit
fixed container migration energy expenditure E_s, E_d	250 mJ
delay associated with wired transmissions T_k^{migr}	2 s
window size to predict incoming traffic W	5 minutes
scheduler time slot τ	3 s
MPC horizon T	{2, 5, 20}
job generation probability p	0.25
weight of the soft constraint penalty c_i of (15)	500
weight of the soft constraint penalty \hat{c}_i of (21)	10
state cost γ for Eq. (14)	100
weight of the quadratic term of (21) ρ	2.5

TABLE IV: Summary of simulation parameters.

algorithm, which is taken from [8], whereas the remaining ones to assess the performance of EASE. For the evaluation, we considered vehicles approaching the edge of the serving eNB coverage area, i.e., that are about to hand over to a new eNB/MEH. With the considered setup, this occurs, on average, when a user is less than 40 meters apart from the radio cell's border. The energy consumption of the MEHs is computed based on the SPECpower benchmark [29]. We selected two different edge computing platforms, namely, an HP ProLiant DL 110 Gen 10 Plus and a Nettrix R620 G40, obtaining two clusters of edge servers with different energy consumption, processing speed and memory, see Table II. In Table III, we report the jobs intensities, deadlines, data sizes, and generation probabilities, according to the system model of Section IV-B. The other system parameters are listed in Table IV.

In the following analysis, we compare our solution against two heuristic strategies: the first, termed “keep” never migrates jobs, which are always and entirely computed by the MEH that received the job processing request in the first place, i.e., the one co-located with the serving eNB at the time when the request was issued. The second heuristic, dubbed “migrate”, whenever a vehicle gets close to the border of its serving eNB, always migrates the associated job to the

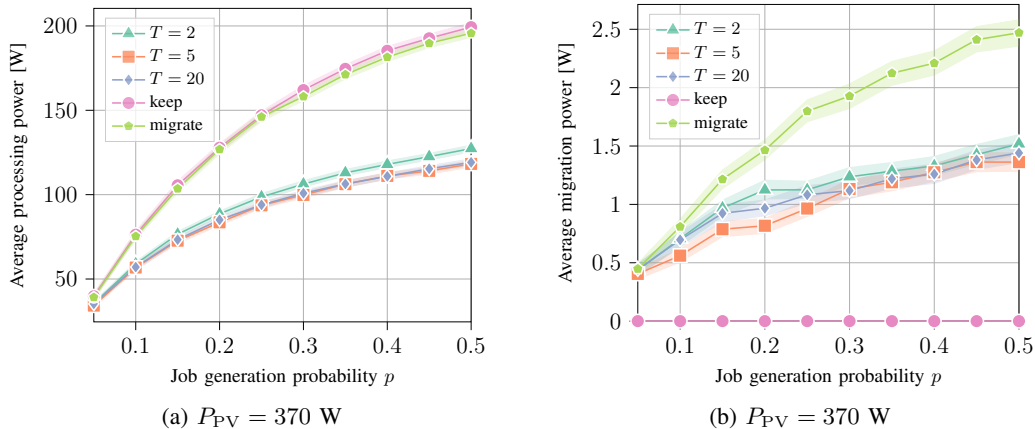


Fig. 3: Average processing (left) and migration (right) power dissipation of the edge servers.

most probable next eNB/MEH among the eNB neighbors.

A. Edge energy consumption

The edge energy consumption is evaluated through the processing and migration power, averaged across the MEHs. In Fig. 3a, the processing power is shown as a function of the job generation probability p . For all the strategies, a concave increase of processing power is observed for an increasing p . The two heuristic policies perform very similarly, draining between 40 to 200 W of power. On the other hand, EASE allows substantial savings, e.g., as much as 80 W at $p = 0.5$ (a gain of 40%). Although two types of servers are used in the simulation, no significant difference is observed regarding the energy consumption induced by the different strategies: the myopic heuristics consume more for both server types. The average power used to migrate the jobs is shown in Fig. 3b. Since the “keep” strategy never migrates tasks, its job migration power is always zero. On the other hand, the strategy with the highest migration power is “migrate”, while the optimized strategies perform in between. Concerning EASE, both processing and migration power depend slightly on the length T of the prediction horizon. A short prediction window, i.e., $T = 2$, has a higher energy consumption due to an imprecise estimation of future resources. The settings $T = 5$ and $T = 20$ lead to the same processing power performance, whereas $T = 20$ uses more migration power (see for, e.g., $p = 0.2$). This reflects the fact that with $T = 20$ the algorithm better captures the future system evolution, thus migrating the jobs to the next serving eNB at a slightly higher rate.

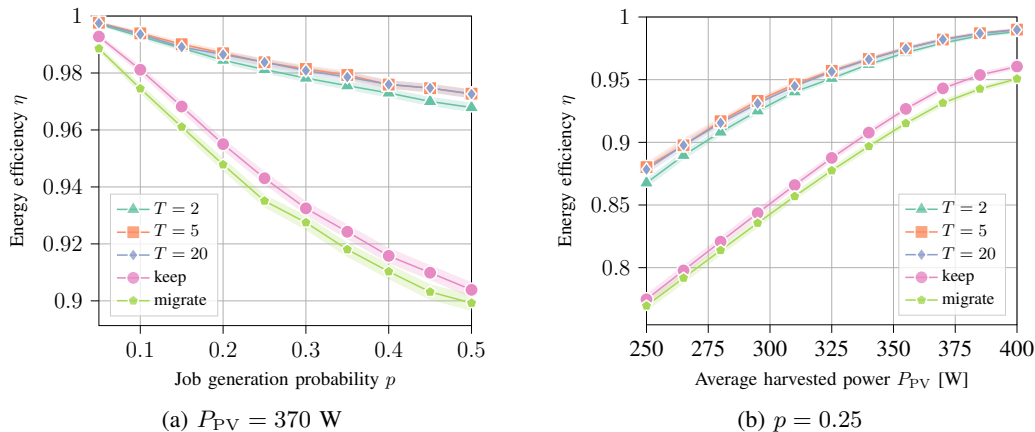


Fig. 4: Energy efficiency with respect to the job generation probability (left) and the power generated by the PV cells (right).

B. Energy and job efficiency

To assess the performance of the scheduling approaches, three metrics are used, namely, i) the energy efficiency, defined as $\eta = E_h/E_{tot}$, i.e., the fraction of harvested (green) energy used over the total energy drained (green plus grid energy), ii) the fraction of executed and finished jobs, and iii) the fraction of jobs finishing in the MEH that is co-located with the eNB serving the vehicle. In Fig. 4a, the energy efficiency η is shown as a function of the job generation probability. All the strategies show an almost linear decrease for increasing p . However, the absolute slope of such decrease is larger for “keep” and “migrate” with respect to EASE. At $p = 0.5$, EASE allows gaining about 7% in efficiency: the harvested energy can fully support the edge network for at least 97% of the total energy requirement. At the same time, EASE almost never discards jobs, while for, e.g., $p \geq 0.3$, the “migrate” and “keep” strategies respectively drop 0.5% and 1.5% of the tasks. The fraction of jobs finishing in the MEH co-located with the eNB providing the connectivity to the vehicle remains nearly constant with respect to p . The “migrate” strategy serves around 75% of the jobs in the same eNB/MEH where the vehicle is, while with EASE this only occurs in about 30% of the cases. This depends on the primary goal of the proposed scheduling pipeline, which corresponds to reducing the carbon footprint of the edge network. As a second-order optimization criterion, and only if feasible, EASE migrates jobs to the next user location (eNB). EASE with $T = 20$ achieves a gain over $T = 5$ of about 2% on this last aspect, while $T = 2$ performs the best, being, however, the least energy efficient. The energy efficiency is also evaluated varying the amount of harvested energy (Fig. 4b), with

the PV panel generating power in $[P_{\min}^{\text{PV}}, P_{\max}^{\text{PV}}]$ W. EASE can entirely sustain the edge at least at 87.5% of the time when the harvested energy is at its minimum, i.e., $P_{\text{PV}} = 250$ W, leading to a gain of 10% with respect to the other strategies, resulting in a significantly reduced carbon footprint. At $P_{\text{PV}} = 400$ W the gain is lower, but EASE performs very close to complete carbon neutrality ($\approx 99\%$ of efficiency). Note that 400 W are just sufficient to self-sustain (on average) the less powerful HP ProLiant server, but not the Nettrix computing unit at full load.

As a final consideration, from Fig. 4 the largest gain is achieved when either the computing demand is high (large p) or the harvested energy is scarce. These are the cases where it is important to use the available resources wisely, and EASE succeeds to do so.

C. Convergence of the dual ascent

In Fig. 5, the convergence speed of the proposed decentralized solution is evaluated. Specifically, the cost value reached at the current iteration is compared with the optimal solution obtained with CVXPY [34], considering the absolute value of their ratio $|\Gamma(\mathbf{x}^+)/\Gamma(\mathbf{x}^*)|$. In the plot, the 90th percentile is shown, discarding hence 10% of outliers. Thus, whenever the ratio settles down to approximately 1, the nodes have reached the global minimum of the cost function. The results show that the power availability impacts the convergence speed: the more harvested energy P_{PV} is available, the quicker the algorithm reaches the minimum. This descends from the fact that a high energy availability leads to a rare activation of the max term in function (18). When the max term returns 0 and the constraint (19) is not active, the optimum is simply given by $\mathbf{o}_i = \bar{\mathbf{w}}_i$, i.e., the selected action is to follow the vehicle movements. The nodes will be very fast in retrieving this particular solution, as the Lagrange multipliers associated with all the constraints remain null after the first two iterations, leading to accept the solution. A similar reasoning holds for the job generation probability that determines the load of the servers. Here, in the interest of space, we omit the associated plot as it is very similar to Fig. 5. Specifically, the convergence requires more iterations as p increases. In fact, an increase in the average load experienced by the servers activates the constraint (19), modifying the optimal solution or even activating the penalties $\hat{\delta}_i$. As it is known, the dual ascent is slow when being close to constraint boundaries. However, as a general result, the number of iterations required to converge even with complex initializations is between 200 and 500. The communication overhead can be evaluated considering that two communication rounds (of few bytes) are required per iteration (see Algorithm 2). Although this may actually appear to be a high number of exchanged messages, we remark that: i) the

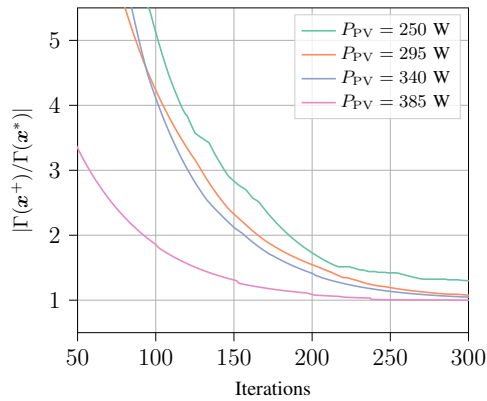


Fig. 5: Ratio between the value of the cost at iteration m and the optimal cost computed with CVXPY (90th percentile). Job generation probability $p = 0.25$.

subsequent step of the proposed pipeline rounds the solution, and, in turn, it is not necessary to retrieve the exact optimum, but it is sufficient to obtain a decent cost value in the continuous domain; ii) we considered slots of $\tau = 3$ s, which is the amount of time available to make a migration decision. Longer time slots can be used, leaving more time to the decision process.

D. Rounding algorithm performance

To test the performance of the rounding Algorithm 3, the cost function (20) is evaluated with the obtained rounded solution $\mathbf{o}^r = \{\mathbf{o}_i^r \mid i \in \mathcal{N}\}$. The comparison is performed with the solution given by each server i simply following the desired $\bar{\mathbf{w}}_i$, i.e., the solution corresponding to the “migrate” strategy. Specifically, the ratio between the cost values of the “migrate” strategy and the rounded solution is computed, considering the cases where it is energetically inefficient to follow the desired migrations. Indeed, in the other case $\mathbf{o}_i = \mathbf{o}_i^r = \bar{\mathbf{w}}_i$, for all servers, i.e., $\bar{\mathbf{w}}_i$ is the optimal solution and it is a feasible one in the discrete domain, thus the costs are equal. As an example, with prediction horizon $T = 5$, job generation probability $p = 0.3$, and $P_{PV} = 300$ W, the gain of using the proposed relax and round optimization procedure of EASE over the “migrate” strategy is on average 10 folds. More in the detail, the gain has a median of 3.8, the 10th percentile is 1.3, meaning that rarely a gain lower than 30% is observed, and the 90th percentile is 17. Hence, often, the rounding step of EASE induces a high gain over the blind “migrate” strategy from an energy perspective.

VIII. CONCLUSIONS

In this paper, we proposed EASE, a novel strategy for online job scheduling in a MEC-enabled network co-powered by the grid and renewable energy resources, considering an IoV scenario.

EASE tackles the problem of ensuring computing service continuity as the users move within the resources-constrained network area. It allows deciding whether to migrate the jobs following the UE, or to continue the execution on the MEC server where it started. This is achieved through the alternation of a local control optimization phase, to estimate future resources, and a distributed consensus step, to reach the migration agreement. The primary objective is the minimization of the carbon footprint at the network side, guaranteeing adequate QoS to the moving users. Using EASE leads to energy efficiency improvements of up to 10% over heuristic strategies, getting close to carbon neutrality in a wide range of contexts.

REFERENCES

- [1] Cisco. (2020) Cisco annual internet report 2018-2023. [Online]. Available: <https://www.cisco.com/c/en/us/solutions/collateral/executive-perspectives/annual-internet-report/white-paper-c11-741490.html>
- [2] *Mobile Edge Computing (MEC); Framework and Reference Architecture*, ETSI Std., Dec. 2020, gS MEC 003 V2.2.1.
- [3] *Multi-access Edge Computing (MEC); MEC 5G Integration*, ETSI Std., Oct. 2020, gS MEC 031 V2.1.1.
- [4] J. Feng, Z. Liu, C. Wu, and Y. Ji, "Mobile edge computing for the internet of vehicles: Offloading framework and job scheduling," *IEEE Vehicular Technology Magazine*, vol. 14, no. 1, pp. 28–36, 2019.
- [5] *Multi-access Edge Computing (MEC); V2X Information Service API*, ETSI Std., Apr. 2020, gS MEC 030 V2.1.1.
- [6] *Multi-access Edge Computing (MEC); Study on MEC Support for V2X Use Cases*, ETSI Std., Sep. 2018, gS MEC 022 V2.1.1.
- [7] *Handover procedures*, 3GPP Std., Sep. 2014, tS 23.009 V12.0.0.
- [8] I. Labriji, F. Meneghello, D. Cecchinato, S. Sesia, E. Perraud, E. C. Strinati, and M. Rossi, "Mobility aware and dynamic migration of MEC services for the internet of vehicles," *IEEE Transactions on Network and Service Management*, vol. 18, no. 1, pp. 570–584, 2021.
- [9] K. Kaur, S. Garg, G. Kaddoum, S. H. Ahmed, and M. Atiquzzaman, "Keids: Kubernetes-based energy and interference driven scheduler for industrial IoT in edge-cloud ecosystem," *IEEE Internet of Things Journal*, vol. 7, no. 5, pp. 4228–4237, 2020.
- [10] T. X. Tran and D. Pompili, "Joint task offloading and resource allocation for multi-server mobile-edge computing networks," *IEEE Transactions on Vehicular Technology*, vol. 68, no. 1, pp. 856–868, 2019.
- [11] M. Feng, M. Krunz, and W. Zhang, "Joint task partitioning and user association for latency minimization in mobile edge computing networks," *IEEE Transactions on Vehicular Technology*, vol. 70, no. 8, pp. 8108–8121, 2021.
- [12] Z. Rejiba, X. Masip-Bruin, and E. Marín-Tordera, "A survey on mobility-induced service migration in the fog, edge, and related computing paradigms," *ACM Comput. Surv.*, vol. 52, no. 5, Sep. 2019.
- [13] T. V. Doan, G. T. Nguyen, H. Salah, S. Pandi, M. Jarschel, R. Pries, and F. H. P. Fitzek, "Containers vs virtual machines: Choosing the right virtualization technology for mobile edge cloud," in *Proceedings of the IEEE 2nd 5G World Forum (5GWF)*, 2019, pp. 46–52.
- [14] S. Ramanathan, K. Kondepu, M. Razo, M. Tacca, L. Valcarenghi, and A. Fumagalli, "Live migration of virtual machine and container based mobile core network components: A comprehensive study," *IEEE Access*, vol. 9, pp. 105 082–105 100, 2021.

- [15] A. Machen, S. Wang, K. K. Leung, B. J. Ko, and T. Salonidis, "Live service migration in mobile edge clouds," *IEEE Wireless Communications*, vol. 25, no. 1, pp. 140–147, 2018.
- [16] L. Ma, S. Yi, N. Carter, and Q. Li, "Efficient live migration of edge services leveraging container layered storage," *IEEE Transactions on Mobile Computing*, vol. 18, no. 9, pp. 2020–2033, 2019.
- [17] A. Aissioui, A. Ksentini, A. M. Gueroui, and T. Taleb, "On enabling 5G automotive systems using follow me edge-cloud concept," *IEEE Transactions on Vehicular Technology*, vol. 67, no. 6, pp. 5302–5316, 2018.
- [18] C. Campolo, A. Iera, A. Molinaro, and G. Ruggieri, "MEC support for 5G-V2X use cases through docker containers," in *Proceedings of IEEE Wireless Communications and Networking Conference (WCNC)*, 2019.
- [19] S. Wang, R. Uргаonkar, M. Zafer, T. He, K. Chan, and K. K. Leung, "Dynamic service migration in mobile edge computing based on markov decision process," *IEEE/ACM Transactions on Networking*, vol. 27, no. 3, pp. 1272–1288, 2019.
- [20] I. Farris, T. Taleb, M. Bagaa, and H. Flick, "Optimizing service replication for mobile delay-sensitive applications in 5g edge network," in *Proceedings of the IEEE International Conference on Communications (ICC)*, Paris, France, May 2017.
- [21] A. Rago, G. Piro, G. Boggia, and P. Dini, "Anticipatory allocation of communication and computational resources at the edge using spatio-temporal dynamics of mobile users," *IEEE Transactions on Network and Service Management*, pp. 1–1, 2021.
- [22] A. Dalgkitis, P.-V. Mekikis, A. Antonopoulos, and C. Verikoukis, "Data driven service orchestration for vehicular networks," *IEEE Transactions on Intelligent Transportation Systems*, vol. 22, no. 7, pp. 4100–4109, 2021.
- [23] W. Zhan, C. Luo, G. Min, C. Wang, Q. Zhu, and H. Duan, "Mobility-aware multi-user offloading optimization for mobile edge computing," *IEEE Transactions on Vehicular Technology*, vol. 69, no. 3, pp. 3341–3356, 2020.
- [24] Q. Yuan, J. Li, H. Zhou, T. Lin, G. Luo, and X. Shen, "A joint service migration and mobility optimization approach for vehicular edge computing," *IEEE Transactions on Vehicular Technology*, vol. 69, no. 8, pp. 9041–9052, 2020.
- [25] G. Perin, M. Berno, T. Erseghe, and M. Rossi, "Towards sustainable edge computing through renewable energy resources and online, distributed and predictive scheduling," *IEEE Transactions on Network and Service Management*, 2021, (early access).
- [26] E. Björnson, J. Hoydis, and L. Sanguinetti, "Massive MIMO networks: Spectral, energy, and hardware efficiency," *Found. Trends Signal Process.*, vol. 11, no. 374, 2017.
- [27] J. Ko, Y. Cho, S. Hur, T. Kim, J. Park, A. F. Molisch, K. Haneda, M. Peter, D. Park, and D. Cho, "Millimeter-wave channel measurements and analysis for statistical spatial channel model in in-building and urban environments at 28 GHz," *IEEE Transactions on Wireless Communications*, vol. 16, no. 9, pp. 5853–5868, 2017.
- [28] H. Liu, C.-Z. Xu, H. Jin, J. Gong, and X. Liao, "Performance and energy modeling for live migration of virtual machines," in *Proceedings of the 20th international symposium on High performance distributed computing*, 2011, pp. 171–182.
- [29] Standard Performance Evaluation Corporation. (2021) SPECpower Results. [Online]. Available: https://www.spec.org/power_ssj2008/results/
- [30] J. B. Rawlings and D. Q. Mayne, *Model predictive control: Theory and design*. Nob Hill Pub., 2009.
- [31] D. P. Bertsekas, *Nonlinear Programming*, 2nd ed. Athena Scientific, 1999.
- [32] D. Krajzewicz, J. Erdmann, M. Behrisch, and L. Bieker, "Recent development and applications of SUMO - Simulation of Urban MObility," *International Journal On Advances in Systems and Measurements*, vol. 5, no. 3&4, pp. 128–138, 2012.
- [33] SUMO. (2021) TAPAS Cologne scenario. [Online]. Available: <https://sumo.dlr.de/docs/Data/Scenarios/TAPASCologne.html>
- [34] S. Diamond and S. Boyd, "CVXPY: A Python-embedded modeling language for convex optimization," *Journal of Machine Learning Research*, vol. 17, no. 83, pp. 1–5, 2016.